Semimagnetic semiconductor quantum wells: magnetic polarons and paramagnetic effects

2000 J. Phys.: Condens. Matter 12 701

(http://iopscience.iop.org/0953-8984/12/5/316)

J. Phys.: Condens. Matter **12** (2000) 701–708. Printed in the UK PII: S0953-8984(00)08185-6

Semimagnetic semiconductor quantum wells: magnetic polarons and paramagnetic effects

T Stirner, M R Farrow and W E Hagston

Department of Physics, University of Hull, Hull HU6 7RX, UK

Received 28 September 1999

Abstract. Photoluminescence experiments were carried out for $Cd_{1-y}Mn_yTe$–$Cd_{1-x}Mn_xTe$–$Cd_{1-y}Mn_yTe$ quantum wells with $y > x$. The magnetic field dependence of the exciton emission lines reveals paramagnetic effects which are markedly different from those of bulk CdMnTe. It is shown that these effects are consistent with a clustering of the Mn ions. Furthermore, at low magnetic fields an additional energy shift in the transition energy is observed. This energy shift can be explained by the formation of exciton magnetic polarons in the quantum wells. The polaron energy is calculated as a function of magnetic field strength and an estimate of the localization radius of the magnetic polaron is made.

1. Introduction

The magneto-optical properties of diluted magnetic semiconductor (DMS) quantum well structures consisting of non-magnetic well material surrounded by semimagnetic barrier material have received a great deal of attention [1]. However, far fewer investigations were concerned with quantum wells consisting of magnetic wells surrounded by magnetic barriers [2–4]. The interest in these systems arises mainly from the large carrier–magnetic ion exchange interaction resulting in Zeeman splittings of the excitonic energy levels of up to several tens of meV. In addition, the polarization of the magnetic ions by the charge carriers can lead to the formation of magnetic polaron complexes [5]. This has implications for the investigation of both the properties of quantum well devices and the fundamentals of the carrier–magnetic ion exchange interaction.

2. Experimental details

The three samples investigated consisted of $Cd_{1-x}Mn_xTe$ well material surrounded by $Cd_{1-y}Mn_yTe$ barriers with $y > x$. The samples were grown by molecular beam epitaxy on (001) InSb substrates followed by a 0.1 μm buffer layer of CdTe. Details of the structural data of the samples are summarized in table 1. Photoluminescence emission experiments were carried out at various external magnetic fields in a superconducting magnet at a temperature of 1.8 K. Details of the sample preparation and the results of photoluminescence excitation and reflectivity measurements on the samples can be found in the literature [2–4].

0953-8984/00/050701+08$30.00

Table 1. Structural details of the samples. L_w denotes the well width, x is the Mn-ion concentration in the well and y the Mn-ion concentration in the barrier region.

Sample	L_w (Å)	x (%)	y (%)
1	150	3.6	9.4
2	140	10.9	16.0
3	75	3.6	9.5

3. Theory

The band gap of $Cd_{1-x}Mn_xTe$ can be either increased or decreased in response to an external magnetic field depending on whether the σ^- or σ^+ optically polarized transitions are observed [6]. The conduction band edge changes by an amount $3A$ and the heavy-hole valence band edge by an amount $3B$ where

$$A = -\frac{1}{6}xN_0\alpha S_0(x)B_J(\boldsymbol{B}, x, T_{\text{eff}}(x))$$

and

$$B = -\frac{1}{6}xN_0\beta S_0(x)B_J(\boldsymbol{B}, x, T_{\text{eff}}(x)).$$

$N_0\alpha$ and $N_0\beta$ are the magnetic exchange constants for the electron and the heavy hole respectively. B_J represents the modified Brillouin function [7] which depends on the external magnetic field $\boldsymbol{B}$, the manganese concentration x and the effective temperature T_{eff}. The effective temperature can be written as the sum of the sample temperature T_{smp} and a semi-phenomenological parameter T_0:

$$T_{\text{eff}}(x) = T_{\text{smp}} + T_0(x).$$

The effective spin S_0 can alternatively be expressed in terms of an effective Mn-ion concentration $\overline{x}$, where

$$\overline{x}S = xS_0(x)$$

and $S = 5/2$. In photoluminescence emission experiments the electronic transitions are associated with the lowest conduction and valence band energy states and one observes a band-gap decrease of $|3A| + |3B|$ in a magnetic field.

The semi-phenomenological parameters $S_0(x)$, the effective spin, and $T_0(x)$, the effective temperature, describe the paramagnetic response of the Mn^{2+} ions to the applied magnetic field. Both parameters have been tabulated for bulk $Cd_{1-x}Mn_xTe$ as a function of x, the Mn-ion concentration [7]. However, recently it was noted that the paramagnetic response of semimagnetic heterostructures, such as quantum wells, is different from that of the bulk. One of these effects was termed 'enhanced paramagnetism' and describes the implications of the lack of translational symmetry at a magnetic–non-magnetic heterojunction interface. Numerical calculations have shown that the latter can change the magnitude of the effective spin at the monolayers near the interface [8, 9]. Another effect was termed 'alloy clustering' and denotes the occurrence of a non-random distribution of the Mn ions in the crystal [10]. Recently a detailed comparison between theoretical calculations and photoluminescence excitation experiments showed that this effect can alter the effective temperature as well as the effective spin of the Mn ions [2].

In order to determine the excitonic transition energies in a magnetic field, the one-particle energies of the electron and the hole, E_e and E_h, were calculated by solving the Schrödinger equation numerically [11]. The exciton binding energies, E_b, were evaluated utilizing the

variational technique developed by Hilton *et al* [12]. The transition energies E_T can then be evaluated using the equation

$$E_T = E_g + E_e + E_h - E_b \tag{1}$$

where E_g denotes the magnitude of the $Cd_{1-x}Mn_xTe$ band gap.

In addition to these 'conventional' paramagnetic effects, the exchange interaction between the magnetic ions and the charge carriers in a DMS can lead to a local polarization of the magnetic ion spins. The resulting complex is called a 'magnetic polaron' [5]. The theoretical formalism employed in the present paper to model magnetic polarons is an extension on the approach to polaron energy calculations first developed by Wolff [13] and described in detail in the literature [14–16]. In short, the method involves minimizing the free energy of the system with respect to the orbital wave function ϕ of the exciton. The system, consisting of a charge carrier with spin $\boldsymbol{s}$ and the magnetic ions with spin $\boldsymbol{S}_j$, can be described by a Heisenberg-type spin Hamiltonian

$$H_{spin} = -J \sum_j \left[\boldsymbol{s} \cdot \boldsymbol{S}_j \, |\phi|^2 \right] \tag{2}$$

where J describes the strength of the spin interaction. Since the number of available spin states of the system is very large, such a Hamiltonian can only be solved for the magnetic polaron energy by employing the partition function of statistical mechanics in order to evaluate an ensemble average over the low-lying energy states [13]. Finally, the change in the exciton binding energy ΔE_b and the kinetic energy of the centre-of-mass motion of the exciton E_{kin} have to be added on to the magnetic polaron energy in order to evaluate the total exciton magnetic polaron energy. Here the kinetic energy term is given by [15]

$$E_{kin} = \frac{\overline{h}^2}{4 M_{xy} R^2} \tag{3}$$

where M_{xy} is the in-plane mass of the exciton and R is the radius of the exciton localization area.

The CdMnTe material parameters employed in the calculations were $m_e^* = 0.096 m_0$ and $m_h^* = 0.6 m_0$ for the effective masses of the electron and hole [17], and $N_0\alpha = 220$ meV and $N_0\beta = -880$ meV for the magnetic exchange parameters of the electron and hole [7] respectively. A valence band offset of 40% was used [18, 19]. The exciton binding energy calculations were performed with a value of the relative permittivity of $\epsilon_r = 10.6$. Following recent experimental and theoretical investigations [1, 20–22], the effective mass of the heavy hole was taken to be isotropic.

4. Results and discussion

Figure 1 shows the excitonic transition energies of samples 1, 2 and 3 as functions of the applied magnetic field. The full circles represent the observed data points obtained by the photoluminescence experiments and the full lines correspond to the theoretical fits. The latter were deduced using a simple model. Based on the fact that the quantum wells are wide, and hence that the energy levels sit near the bottom of the well, we can, as a first approximation, consider the changes in E_g only in a magnetic field [7]. As a result, the shift of the quantum well energy level can be compared to the shift of a 'hypothetical' bulk magnetic layer with Mn-ion concentration x. The magnetic field dependence of this shift can be described by the equation

$$\Delta E = \frac{1}{2} x N_0 (\beta - \alpha) S_0 B_J(\boldsymbol{B}, x, T_{eff}(x)) \tag{4}$$

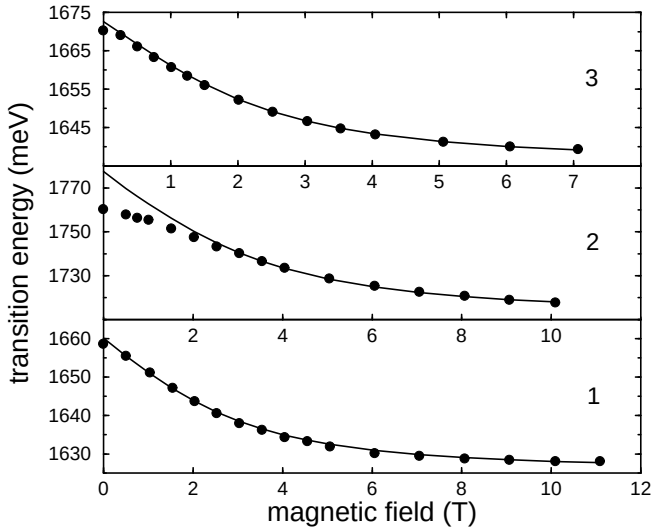

Figure 1. Magnetic field dependences of the exciton transition energies for samples 1, 2 and 3 at $T = 1.8$ K. The full circles represent the experimental data points and the full lines are modified Brillouin function fits.

where S_0 and T_0 act as fitting parameters. Table 2 shows the fitting parameters which were employed in obtaining the Brillouin function curves in figure 1. Also shown in table 2 are the bulk values of the effective spin and temperature for the well and barrier layers of samples 1 to 3.

Table 2. Values for the effective spin S_0 and effective temperature T_0 used in equation (4) to fit the observed exciton energy shifts in figure 1. Also shown are the bulk values of S_0 and T_0 (taken from reference [7]) for x and y as in table 1. T_0 is in units of K.

Sample	S_0	$S_0(x)$	$S_0(y)$	T_0	$T_0(x)$	$T_0(y)$
1	1.685	1.679	1.056	3.98	1.257	2.671
2	1.050	0.946	0.671	5.00	2.955	3.751
3	1.800	1.679	1.048	3.00	1.257	2.691

As can be seen from table 2, the effective spin values used in the modified Brillouin function fitting procedure agree quite well with the corresponding bulk values of the well layers. This is to be expected since the well layers are relatively wide, and hence the energy shift of the excitonic state follows closely the change in band gap of the well material. However, one can also see from table 2 that the value of the effective temperature is significantly higher than the values determined for bulk. As will be shown below, we attribute this behaviour to the effects of alloy clustering.

A further feature that can be observed from figure 1 is a deviation of the experimental data values from the Brillouin function curves at low magnetic field values. This additional energy shift is suppressed with increasing magnetic field and can be attributed to the formation of magnetic polarons in the quantum well regions. The formation of magnetic polarons occurs in all three samples; however, the effect is more pronounced in sample 2 which has the largest Mn-ion concentration in the well region. The zero-field exciton magnetic polaron energies as determined from figure 1 are 1.5, 17.1 and 2.3 meV for samples 1, 2 and 3 respectively. In

this context we note that the zero-field reflectivity for sample 2 was observed at an energy of 1777.9 meV, giving an energy separation of 17.5 meV between the photoluminescence and reflectivity peaks of this sample.

Figure 2 shows the same experimental data points as figure 1; however, the theoretical lines were generated now by evaluating equation (1) exactly. For comparison, the dashed lines in figure 2 were produced using bulk values of the effective temperature. With regard to the theoretical fitting procedure in figure 2 we note two main points. First, the magnitudes of the Zeeman splittings at saturation can be reasonably well reproduced with the bulk values of the effective spin for samples 1 and 3. Only for sample 2 was it necessary to introduce a slightly larger value of the effective Mn-ion concentration in the well region (of 0.0458). This enhancement can be attributed to enhanced paramagnetism effects associated with the larger concentration values. Second, as can be seen from the dashed lines in figure 2, there is a marked discrepancy between theory and experiment at intermediate magnetic fields, for the curves generated using bulk values of the effective temperature. This same effect has also been observed in these samples in the photoluminescence excitation spectra [2]. We attribute this behaviour to the occurrence of alloy clustering, which gives rise to an enhancement in the effective temperature values compared with the corresponding values for bulk material. The full lines in figure 2 show the theoretical results associated with the enhanced values of T_0 in the well regions of the samples. The corresponding values of T_0 employed in the calculations for samples 1, 2 and 3 were 3.3, 4.7 and 2.1 K respectively. These values have to be compared with the bulk values quoted in table 2. We note that the additional energy shifts due to magnetic polaron formation are again visible at low magnetic fields in figure 2.

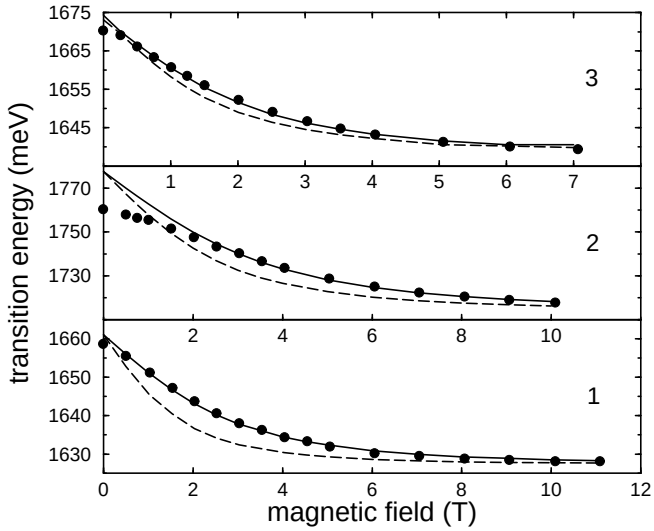

Figure 2. Magnetic field dependences of the exciton transition energies as in figure 1. The full (dashed) lines represent the theoretical calculations including (ignoring) alloy clustering effects.

We now turn to the evaluation of the exciton magnetic polaron energies. Here we focus our attention on sample 2 since, as can be seen from figures 1 and 2, its polaron energy is significantly larger than those of samples 1 and 3. Figure 3 shows the exciton magnetic polaron (EMP) energy as a function of the localization radius of the centre-of-mass motion of the exciton. The three full curves in figure 3 were generated with bulk values for the effective spin and temperature (labelled 'bulk'), an enhanced value of the effective spin (of 1.05 and

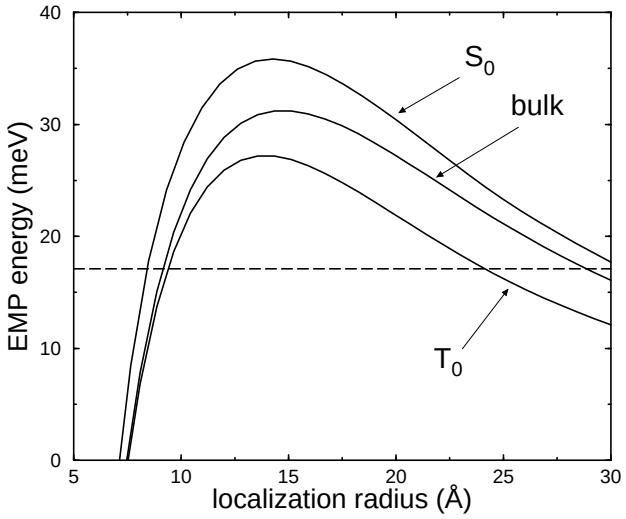

Figure 3. Exciton magnetic polaron energy as a function of localization radius for sample 2 ($\boldsymbol{B} = 0$ T, $T = 1.8$ K). The full lines represent the theoretical calculations for the $Cd_{1-x}Mn_xTe$ well layer responding like bulk, with enhanced effective spin S_0 and enhanced effective temperature T_0. The dashed line shows the experimentally observed EMP energy.

labelled 'S_0') and an enhanced value of the effective temperature (of 5.0 K and labelled 'T_0'; see also table 2). Also shown in figure 3 by the dashed line is the experimentally determined value of the EMP energy of 17.1 meV for sample 2 at zero magnetic field. There are several points to note. Whereas an enhancement in the effective spin gives rise to increased EMP energies, an enhanced effective temperature results in decreased EMP energies. The net result is a partial cancellation of the two effects, and the resulting curve, which agrees with the experimental results in figure 2, is virtually identical to the curve labelled 'bulk'. Furthermore, the observed EMP energy is significantly smaller than the maximum theoretically possible EMP energy for this quantum well. A possible explanation for this behaviour is that in our quantum wells the polaron formation times are significantly longer than the exciton recombination times, i.e. the polarons may not have enough time to form fully. This explanation is also consistent with experimental results on $Cd_{1-x}Mn_xTe$ epilayers where it was observed [23] that the polaron formation process is interrupted by the recombination of the excitons for $x < 0.17$.

Figure 4 shows the magnetic field dependence of the EMP energy for sample 2. The experimentally observed polaron energies, shown by the full circles in figure 4, are fully suppressed by an external field of $\approx$3.5 T. The full line in figure 4 shows the results of the theoretical calculations. The localization radius employed in the calculations in order to obtain agreement with the observations is shown in the inset to figure 4. The localization radius at zero magnetic field was taken to be 9 Å (see figure 3). As can be seen from the inset to figure 4, external magnetic fields below $\approx$2 T do not change significantly the in-plane localization of the exciton wave function. However for larger magnetic fields the centre-of-mass motion of the exciton becomes increasingly more delocalized.

5. Summary

The photoluminescence spectra of three $Cd_{1-y}Mn_yTe$–$Cd_{1-x}Mn_xTe$–$Cd_{1-y}Mn_yTe$ quantum wells with $y > x$ were analysed theoretically. The magnetic field dependence of the exciton

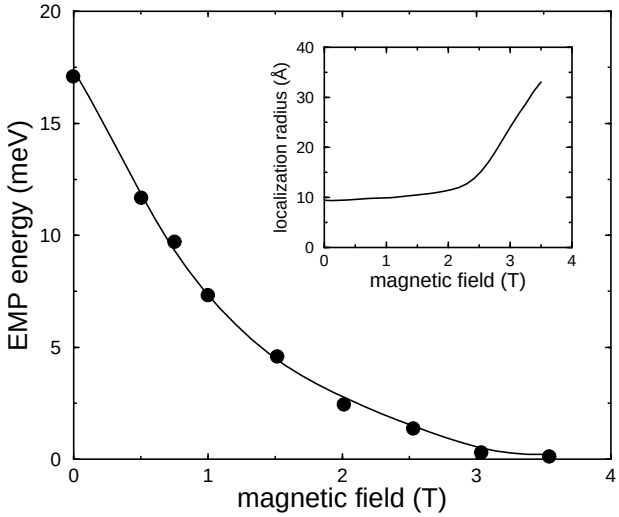

Figure 4. The magnetic field dependence of the exciton magnetic polaron energy for sample 2. The full circles represent the experimental data points and the full line the theoretical calculations employing the localization radii as shown in the inset.

emission lines revealed two main features. First, comparing the experimental observations with calculations using bulk values for the paramagnetic response parameters of the manganese ions showed a marked discrepancy between theory and experiment at intermediate magnetic fields. This behaviour was attributed to alloy clustering effects leading to an enhancement of the effective temperature. In general, the amount of clustering will depend on the conditions during a molecular-beam-epitaxy growth run. The dimensional details of the clustering however are difficult to determine with magneto-optical experiments, since the exciton wave functions extend over several tens to hundreds of angströms. Second, at low magnetic fields an additional energy lowering was observed. This energy shift is suppressed by the application of an external magnetic field and can be attributed to the formation of magnetic polarons in the quantum wells. Calculations of the polaron energy showed that the exciton localization radius is of the order of 10 to 30 Å at zero magnetic field and increases with increasing magnetic field.

Acknowledgments

The authors would like to thank S J Weston and J E Nicholls for the results of photoluminescence measurements.

References

[1] See, e.g., Jackson S R, Nicholls J E, Hagston W E, Harrison P, Stirner T, Hogg J H C, Lunn B and Ashenford D E 1994 *Phys. Rev.* B **50** 5392 and references therein
[2] Weston S J, O'Neill M, Nicholls J E, Miao J, Hagston W E and Stirner T 1998 *Phys. Rev.* B **58** 7040
[3] Weston S J, Stirner T, Harrison P, Nicholls J E, Hagston W E and Ashenford D E 1993 *J. Physique Coll.* IV C5 **3** 397
[4] Weston S J 1995 *PhD Thesis* University of Hull
[5] Mackh G, Ossau W, Yakovlev D R, Waag A, Litz T and Landwehr G 1993 *Solid State Commun.* **88** 221
[6] Willardson R K and Beer A C (ed) 1988 *Diluted Magnetic Semiconductors (Semiconductors and Semimetals vol 25)* (London: Academic)

[7] Gaj J A, Planel R and Fishman G 1979 *Solid State Commun.* **29** 435
Gaj J A, Bodin-Deshayes C, Peyla P, Cibert J, Feuillet G, Merle d'Aubigne Y, Romestain R and Wasiela A 1992 *Proc. 21st Int. Conf. on the Physics of Semiconductors* (Singapore: World Scientific) p 1936
[8] Fatah J M, Piorek T, Harrison P, Stirner T and Hagston W E 1994 *Phys. Rev.* B **49** 10 341
[9] Stirner T, Fatah J M, Roberts R G, Piorek T, Hagston W E and Harrison P 1994 *Superlatt. Microstruct.* **16** 11
[10] Harrison P, Fatah J M, Stirner T and Hagston W E 1996 *J. Appl. Phys.* **79** 1684
[11] Harrison P, Hagston W E and Stirner T 1993 *Phys. Rev.* B **47** 16 404
[12] Hilton C P, Goodwin J, Harrison P and Hagston W E 1992 *J. Phys. A: Math. Gen.* **25** 5365
[13] Wolff P A 1988 *Diluted Magnetic Semiconductors (Semiconductors and Semimetals vol 25)* ed R K Willardson and A C Beer (London: Academic) p 413
[14] Hagston W E, Stirner T, Goodwin J P and Harrison P 1994 *Phys. Rev.* B **50** 5255
[15] Stirner T, Hagston W E, Harrison P and Goodwin J P 1994 *J. Appl. Phys.* **75** 3466
[16] Stirner T and Hagston W E 1996 *J. Appl. Phys.* **80** 2339
[17] Dang L S, Neu G and Romestain R 1982 *Solid State Commun.* **44** 1187
[18] Chen P, Nicholls J E, Hogg J H C, Stirner T, Hagston W E, Lunn B and Ashenford D E 1995 *Phys. Rev.* B **52** 4732
[19] Mackh G, Hilpert M, Yakovlev D R, Ossau W, Heinke H, Litz T, Fischer F, Waag A, Landwehr G, Hellmann R and Göbel E O 1994 *Phys. Rev.* B **50** 14 069
[20] Haines M J L S, Ahmed N, Adams S J A, Mitchell K, Agool I R, Pidgeon C R, Cavenett B C, O'Reilly E P, Ghiti A and Emeny M T 1991 *Phys. Rev.* B **43** 11 944
[21] Stirner T, Harrison P, Hagston W E and Goodwin J P 1994 *Phys. Rev.* B **50** 5713
[22] Harrison P, Long F and Hagston W E 1996 *Superlatt. Microstruct.* **19** 123
[23] Mackh G, Ossau W, Yakovlev D R, Waag A, Landwehr G, Göbel E O and Hellmann R 1994 *Phys. Rev.* B **49** 10 248